ACS OMEGA

http://pubs.acs.org/journal/acsodf

Article

Initial Thermal Decomposition Mechanism of $(NH_2)_2C{=}C(NO_2)(ONO)$ Revealed by Double-Hybrid Density Functional Calculations

Yulei Guan,* Xingzhen Zhu, Yanyan Gao, Haixia Ma, and Jirong Song

Cite This: *ACS Omega* 2021, 6, 15292−15299

Read Online

ACCESS | Metrics & More | Article Recommendations | Supporting Information

ABSTRACT: This work employs double-hybrid density functionals to re-examine the CO−NO bond dissociation mechanism of nitrite isomer of 1,1-diamino-2,2-dinitro-ethylene (DADNE) into $(NH_2)_2C{=}C(NO_2)O$ and nitric monoxide (NO). The calculated results confirm that an activated barrier is present in the CO−NO bond dissociation process of $(NH_2)_2C{=}C(NO_2)$-(ONO). Furthermore, it is proposed that a radical−radical adduct is involved in the exit dissociation path with subsequent dissociation to separate $(NH_2)_2C{=}C(NO_2)O$ and NO radicals. The activation and reaction enthalpies at 298.15 K for the nitrite isomer dissociation are predicted to be 43.6 and 5.4 kJ mol^{-1} at the B2PLYP/6-31G(d,p) level, respectively. Employing the B2PLYP/6-31G(d,p) reaction energetics, gradient, Hessian, and geometries, the kinetic model for the CO−NO bond dissociation of $(NH_2)_2C{=}C(NO_2)(ONO)$ is obtained by a fitting to the modified Arrhenius form $1.05 \times 10^{13}(T/300)^{0.39}$ $\exp[-27.80(T + 205.32)/R(T^2 + 205.32^2)]$ in units of per second over the temperature range 200−3000 K based on the canonical variational transition-state theory with multidimensional small-curvature tunneling.

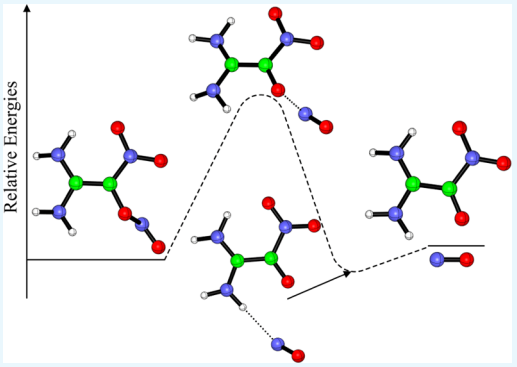

INTRODUCTION

Over the last decade, there has been a significant effort to develop new candidates, which might lead to improved explosives in terms of performance, safety, and other favorable properties.[1−3] 1,1-Diamino-2,2-dinitro-ethylene (DADNE), also called FOX-7, which is described as a push−pull ethylene with two donating amine groups and two withdrawing nitro groups, is an insensitive high-density energetic material, which makes it a promising and potentially useful replacement for the currently widely used energetic materials.[4,5] To gain insight into these characteristics, it is necessary to understand its thermolysis mechanism.

Considerable decomposition work has been performed with DADNE to determine its properties as a promising type of explosive.[6−8] However, few experimental studies have been performed on the possible decomposition pathways of DADNE, and the chemical initiation mechanism of thermolysis is often simply attributed to the dissociation of the weakest C−NO_2 bond. There have been also several quantum chemical calculations[9−14] to predict the unimolecular thermolysis processes of DADNE, with a focus on discovering the lowest-energy decomposition pathway. The initial decomposition reactions were found to proceed via four distinct pathways in the gas phase, depicted as in Figure 1: direct C−NO_2 bond fission with NO_2 loss (R1), NO loss via a nitro-nitrite rearrangement and further CO−NO bond dissociation (R2), intramolecular isomerization to $(NH)(NH_2)C{=}C(NO_2)(NO_2H)$, followed by cyclization and subsequent water elimination (R3), and enamine-to-imine isomerization (a hydrogen transfer from an amine to the nitro-carbon atom) with the subsequent C−NO_2 bond fission to yield $(NH)(NH_2)C{-}C(H)(NO_2)$ + NO_2 (R4).

NO loss via nitro-nitrite isomerization is considered to be the most important of the four possible initial steps in the DADNE decomposition since reaction R2 not only is the most energetically favored initial step to trigger the decomposition of DADNE with the fact that NO was detected experimentally as the most abundant primary dissociation product;[13,14] it also leads to radical intermediates that undergo net exothermic product channels. In addition, due to the ethene substructure in the nitrite isomer of DADNE, $(NH_2)_2C{=}C(NO_2)(ONO)$, its CO−NO bond dissociation may be considerably different from that for alkanes and deserves further study. Up to now, experimental and theoretical information on the detailed mechanisms of the title reaction was very limited. The CO−NO bond dissociation of $(NH_2)_2C{=}C(NO_2)(ONO)$ to produce $(NH_2)_2C{=}C(NO_2)O$ and NO radicals was previously assumed to be "barrierless", and the process for $(NH_2)_2C{=}C(NO_2)O$ and NO radical recombination occurred without a barrier.[10−13] Interestingly, recent theoretical

Received: March 25, 2021
Accepted: May 21, 2021
Published: June 3, 2021

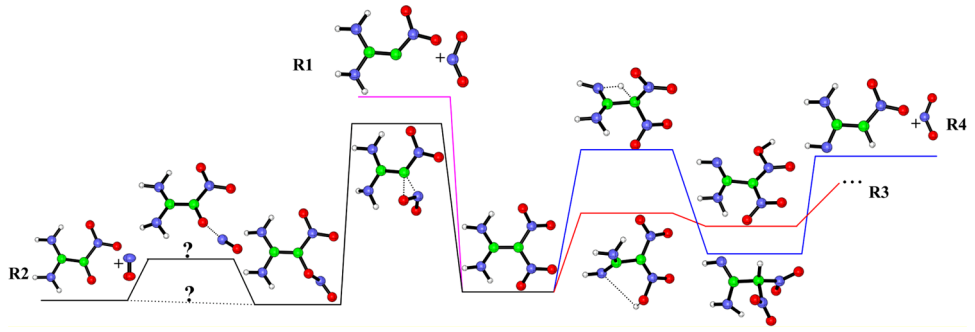

Figure 1. Four initial decomposition channels of DADNE on the ground-state potential energy surface. Color code of atoms: red, oxygen; blue, nitrogen; green, carbon; and white, hydrogen.

calculations by Booth and Butler[14] proposed that there existed a barrier of about 61 kJ mol^{-1} calculated at the G4//B3LYP/6-311++G(3df,2p) level to be surmounted for the CO−NO bond dissociation of nitrite isomer. From the above discussion, one can see that the mechanism of the initial thermolysis stages of $(NH_2)_2C{=}C(NO_2)(ONO)$ still remains unclear, as described in Figure 1.

In light of the uncertainties in the CO−NO bond rupture of nitrite isomer, determining whether the reaction process involves a transition state or not is of considerable interest. Even a low-barrier height would affect the decomposition rate constant significantly and make a crucial difference to interpret the experimental results. In addition, it is long known that quantum mechanical effects in the vicinity of the transition state showed a strong influence on the state-to-state reaction dynamics. Therefore, exploring the underlying reactivity of nitrite isomer is the key point for improving the decomposition model of DADNE.

The study presented here computationally investigates this strange behavior for the NO-loss pathway of $(NH_2)_2C{=}C(NO_2)(ONO)$. Ab initio molecular orbital theory is employed to detail the energetic profile of the CO−NO bond dissociation pathway of $(NH_2)_2C{=}C(NO_2)(ONO)$ via "double-hybrid" density functional calculations to verify whether or not a well-defined transition state is involved in the title reaction. High-pressure thermal rate constants are estimated in the temperature range of 200−3000 K based on canonical variational transition-state theory including multi-dimensional tunneling corrections.

RESULTS AND DISCUSSION

Nitrite Isomers of DADNE. After nitro to nitrite isomerization of DADNE, the nitrite isomer, $(NH_2)_2C{=}C(NO_2)(ONO)$, has two conformers, trans and cis, with respect to the carbon atom linked to the nitrite moiety. The trans and cis conformers can interconvert to each other with the N4O4 group rotating around the O3−N4 bond. Figure 2 depicts the minimum-energy path by rotating the dihedral angle O4N4O3C2 from 0 to 360° with 10° increments by a relaxed scan optimization algorithm. *cis*-$(NH_2)_2C{=}C(NO_2)(ONO)$ is found to be deep minima compared to the trans conformation, perhaps due to weak $\pi-\pi$ interactions between the −ONO group and the C=C double bond.

A transition state, $TS_{cis\text{-}trans}$, presenting an imaginary frequency, i.e., 236*i* cm^{-1} at the B2PLYP/6-31G(d,p) level, for the rotation of the N4O4 moiety around the O3−N4 axis has been identified, in which the dihedral angle O4N4O3C2 is located to be about 78°. The required barrier height is

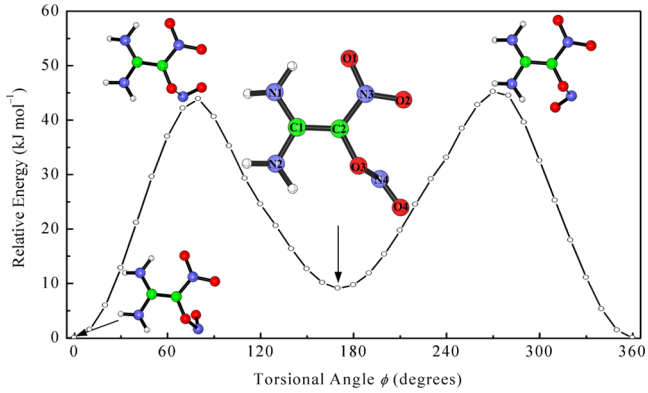

Figure 2. One-dimensional potential for the rotation of the N4O4 group about the O3−N4 bond of the nitrite isomer of DADNE calculated at the B2PLYP/6-31G(d,p) level. Color code of atoms: red, oxygen; blue, nitrogen; green, carbon; and white, hydrogen.

predicted to be 40−41 kJ mol^{-1} for the process of cis to trans conformer, as listed in Table S1, along with an obvious elongation of the O3−N4 bond by 0.077 and 0.188 Å calculated at the B2PLYP/6-31G(d,p) level compared to cis and trans conformers, respectively, indicating that it suffers a loose rotation of the N4O4 group about the O3−N4 bond.

Because the nitro to nitrite isomerization of DADNE is ready to produce the trans-nitrite isomer, and compared to the subsequent O3−N4 bond dissociation, a considerable barrier to be overcome separates cis- and trans-nitrite isomers; the subsequent discussions are all about the O3−N4 bond dissociation of the trans-nitrite isomer of DADNE, although the trans conformer has higher energy than the cis-conformer by 8−11 kJ mol^{-1}, as shown in Table S1.

Potential Energy Surface for the CO−NO Bond Rupture. The nitrite isomer of DADNE has an elongated O3−N4 bond (~1.6 Å), which is very weak and undergoes bond dissociation. NBO calculations show that despite the long bond length, the O3−N4 bond retains two electrons, rather than a biradical form. In an effort to obtain a better understanding of the O3−N4 bond dissociation of nitrite isomer, the optimized potential energy surface for $(NH_2)_2C{=}C(NO_2)(ONO) \rightarrow (NH_2)_2C{=}C(NO_2)O + NO$, as shown in Figure 3, is obtained at the B2PLYP/6-31G(d,p) level by optimizing the geometry at a series of fixed distances between O3 and N4 atoms from 1.594 to 4.094 Å with the spin multiplicity as 1. The B2PLYP/6-31G(d,p) dissociation curves for $(NH_2)_2C{=}C(NO_2)(ONO) \rightarrow (NH_2)_2C{=}CONO + NO_2$ and $(NH_2)_2C{=}C(NO_2)_2 \rightarrow (NH_2)_2C{=}CNO_2 + NO_2$ with the distance between the bonding C and N atoms are also

https://doi.org/10.1021/acsomega.1c01616
ACS Omega 2021, 6, 15292−15299

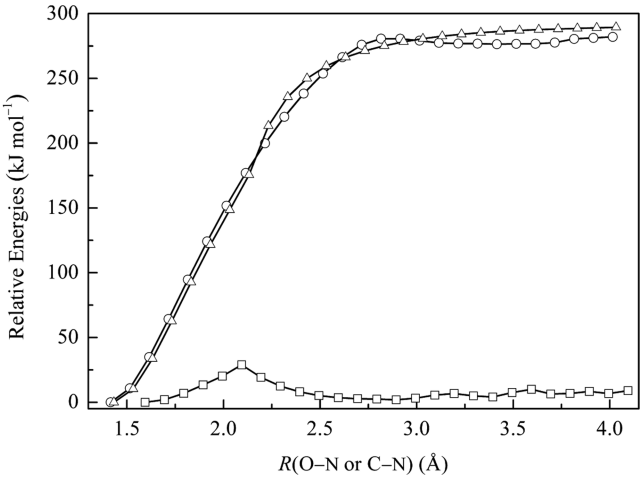

Figure 3. Fully optimized B2PLYP/6-31G(d,p) potential energy curves for the O3−N4 bond (in squares) and the C−NO_2 bond (in circles) ruptures of nitrite isomer $(NH_2)_2C{=}C(NO_2)(ONO)$ and C−NO_2 bond (in triangles) scission of DADNE.

depicted in Figure 3 for comparison. One can observe that the energies of the $[(NH_2)_2C{=}C(ONO)\cdots NO_2]$ and $[(NH_2)_2C{=}C(NO_2)\cdots NO_2]$ systems increase first with the C−NO_2 bond length and eventually reach a plateau, involving no tight transition state along the reaction coordinates.

The relative energy of $(NH_2)_2C{=}CNO_2$ + NO_2 to $(NH_2)_2C{=}C(NO_2)_2$ is calculated to be 302.9 kJ mol^{-1} at the B2PLYP/6-31G(d,p) level without the ZPE correction. After ZPE and thermal corrections to enthalpy, this energy value is reduced to 290.5 kJ mol^{-1} at 298.15 K, which is in reasonable agreement with the previous B3P86/6-31+G(d,p) calculated result[9] by 292.9 kJ mol^{-1} and G4//B3LYP/6-311++g(3df,2p) value[14] by 290.0 kJ mol^{-1}, indicating that the adopted double-hybrid density functionals are reasonable to characterize the title reaction. As seen from Figure 3, it is interesting to note that there exists a maximum point in energy in the homolytic cleavage process of the CO−NO bond of $(NH_2)_2C{=}C(NO_2)(ONO)$, and there is a strong possibility that the geometry with peak potential energy is a transition state. Here, it can be argued that the decomposition of $(NH_2)_2C{=}C(NO_2)(ONO)$ shows similar behavior to the CO−NO bond scission of vinyl nitrite.[15] Furthermore, $(NH_2)_2C{=}C(NO_2)(ONO)$ immediately dissociates via the CO−NO bond scission to generate $(NH_2)_2C{=}C(NO_2)O$ + NO upon nitrite isomer formation. This is a result of the much weaker CO−NO bond relative to the C−NO_2 bonds of $(NH_2)_2C{=}C(NO_2)(ONO)$ and DADNE.

Geometric Structures and Energies. We next verify that the B3LYP/6-311++G(3df,2p)-based transition state by Booth and Butler[14] was not an artifact. The double-hybrid density functionals B2PLYP, B2PLYPD, B2PLYPD3, mPW2PLYP, and mPW2PLYPD in combination with the 6-31G(d,p) basis set are employed to find the transition state for the CO−NO dissociation of $(NH_2)_2C{=}C(NO_2)(ONO)$ via the "TS" and "QST3" using a broken-symmetry unrestricted formalism with the "Guess = Mix" keyword implemented as in Gaussian 09 software, and a tight NO-loss transition state is located.

Figure 4 depicts the optimized geometries of the stationary points at the B2PLYP/6-31G(d,p) level, and Table S2 in the Supporting Information compares the selected geometrical parameters obtained with various double-hybrid density

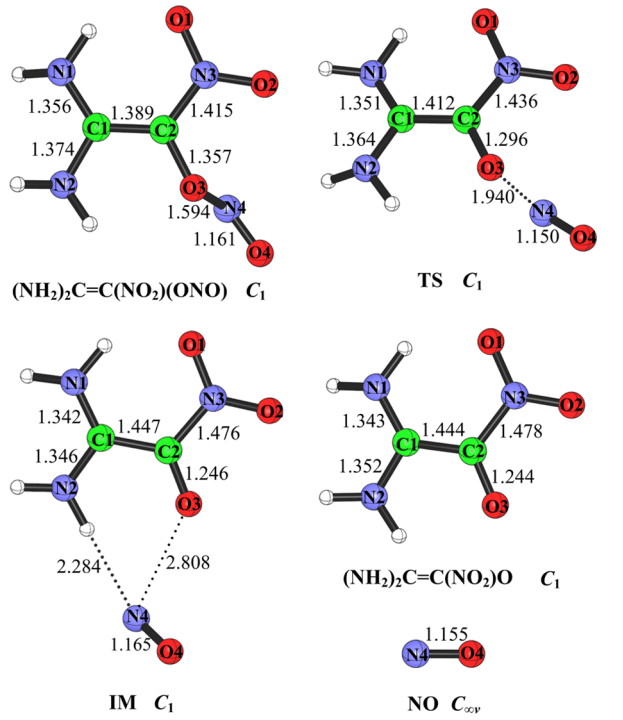

Figure 4. Optimized geometries of the reactant, transition state (TS), intermediate (IM), and products for the CO−NO bond dissociation of $(NH_2)_2C{=}C(NO_2)(ONO)$ to form $(NH_2)_2C{=}C(NO_2)O$ + NO at the B2PLYP/6-31G(d,p) level. The carbon atoms are shown in green, oxygen in red, nitrogen in blue, and hydrogen in white.

functionals and a good agreement is achieved. Details of electronic geometries, rotational constants, and unscaled vibrational frequencies at different theoretical levels for all species are also supplied in the Supporting Information.

All adopted double-hybrid density functionals give essentially the same results for the lengths of the breaking CO−NO bond in the optimized transition structures, i.e., 1.940, 1.939, 1.940, 1.920, and 1.920 Å, respectively, at the B2PLYP, B2PLYPD, B2PLYPD3, mPW2PLYP, and mPW2PLYPD levels with the 6-31G(d,p) basis set, as shown in Table S2, which is in good agreement with the B3LYP/6-311++g(3df,2p) based value of 1.99 Å.[14] The located transition state is identified as the first-order saddle point by only one imaginary frequency, which corresponds to the process of combination and separation of the $(NH_2)_2C{=}C(NO_2)O$ and NO moieties. Furthermore, the IRC calculations confirm that the title reaction should follow a direct path from the nitrite isomer minimum-energy geometry via the transition state TS to a hydrogen-bonded $(NO_2)C{=}C(NH_2)NH\cdots H\cdots NO$ radical−radical complex (IM) on the product side, rather than dissociate to the free products. This means it is improper to treat the $(NH_2)_2C{=}C(NO_2)(ONO)$ → $(NH_2)_2C{=}C(NO_2)O$ + NO reaction without an activation barrier. In the TS geometry, the structural parameters of the $(NH_2)_2C{=}C(NO_2)O$ and NO parts are almost the same as those in their individual structures obtained at the same theoretical level, implying a weak interaction between $(NH_2)_2C{=}C(NO_2)O$ and NO moieties.

The evaluation of the global electron density transfer (GEDT) in the title reaction is made by means of electrostatic Hirshfeld population analysis.[16] The Hirshfeld population analysis of the TS yields a GEDT flux of only 0.03e for the

https://doi.org/10.1021/acsomega.1c01616
ACS Omega 2021, 6, 15292−15299

Table 1. Relative ZPE-Corrected[a] Entropies (ΔS, in J mol^{-1} K^{-1}), Energies, Enthalpies, and Free Energies (ΔE, ΔH, and ΔG in kJ mol^{-1}) at 298.15 K of the Involved Stationary Points to Reactant in the CO−NO Bond Dissociation of $(NH_2)_2C{=}C(NO_2)(ONO)$

species	electronic model chemistry	ΔE	ΔS	ΔH	ΔG
TS	B2PLYP	43.1	8.4	43.6	41.0
	B2PLYPD	43.2	9.1	43.7	41.0
	B2PLYPD3	42.9	9.0	43.4	40.7
	mPW2PLYP	40.8	9.0	41.4	38.7
	mPW2PLYPD	40.9	9.4	41.5	38.7
IM	B2PLYP	−8.9	74.4	−3.5	−25.7
	B2PLYPD	−7.9	74.9	−2.5	−24.9
	B2PLYPD3	−7.1	75.1	−1.8	−24.2
	mPW2PLYP	−13.1	69.2	−8.0	−28.6
	mPW2PLYPD	−12.3	69.4	−7.3	−28.0
$(NH_2)_2C{=}C(NO_2)O$ + NO	B2PLYP	2.3	163.6	5.4	−43.4
	B2PLYPD	6.4	164.3	9.6	−39.4
	B2PLYPD3	6.9	163.7	10.0	−39.7
	mPW2PLYP	1.9	165.3	5.2	−44.1
	mPW2PLYPD	2.9	165.8	6.3	−43.1

[a]ZPEs are scaled.

transferred electron density from the nucleophilic $(NH_2)_2C{=}C(NO_2)O$ moiety toward the electrophilic NO unit, which shows that this reaction has a nonpolar character.

As mentioned above, the CO−NO bond dissociation of singlet $(NH_2)_2C{=}C(NO_2)(ONO)$ proceeds via a spin-flip process to produce two doublet radicals, introducing variation in electron correlation where two electrons initially paired in the CO−NO bonding orbital become separated into two different orbitals. This has important consequences for the TS structure, which contains an elongated bond and may contain both singlet and triplet spin states, suffering from the problem of spin contamination. Furthermore, $(NH_2)_2C{=}C(NO_2)O^{\bullet} \leftrightarrow {}^{\bullet}C(NH_2)_2{-}C{=}O(NO_2)$ isomerization (the dot $^{\bullet}$ stands for radical center) indicates that the $(NH_2)_2C{=}C(NO_2)O$ radical has two resonantly stabilized structures, with the latter being prominent, which is supported by the WBO values of 1.38 and 1.00 at the breaking C=C and the forming C=O bonds in $(NH_2)_2C{=}C(NO_2)(ONO)$ and 1.15 and 1.45 in the $(NH_2)_2C{=}C(NO_2)O$ radical, respectively. Therefore, it is necessary to assess whether the single-reference treatments are suitable for an accurate description of the title reaction. To evaluate the multiple reference character in the wave functions of the reactant, intermediate, and transition state, T1 diagnostic[17] from the CCSD[18,19]/6-31+G(d,p) calculations on the B2PLYP/6-31G(d,p)- and mPW2PLYP/6-31G(d,p)-based geometries and $\langle S^2\rangle$ examinations for open-shell species are implemented, and the calculated results are summarized in Table S3.

Examining Table S3, we can see that the T1 diagnostic parameters obtained for TS, IM, $(NH_2)_2C{=}C(NO_2)O$, and NO, which suffer from spin contamination, appear to be relatively high, but they may still be considered to be uncritical compared to the open-shell cutoff T1 value of 0.045 for multiple reference character[20] and that for the spin-restricted geometry $(NH_2)_2C{=}C(NO_2)(ONO)$ is calculated to be just a little larger than the benchmark value of 0.02 for the closed-shell systems.[17] In addition to the T1 diagnostic concerns, the deviations of $\langle S^2\rangle$ values from 0.75 and 2.0 are found to be very small for the $(NH_2)_2C{=}C(NO_2)O$ and NO doublet state and the IM triplet state, respectively. Here, it can be argued that the single-reference-based electron correlation procedure can reliably treat the present case based on $\langle S^2\rangle$ and T1 diagnostic values. The predicted harmonic vibrational frequencies and rotational moments of inertia for the reactant and TS are shown in the Supporting Information and applied for calculating the rate constants and other kinetic parameters. Our calculated values of the vibrational frequencies for $(NH_2)_2C{=}C(NO_2)(ONO)$ are compared with the previous B3P86/6-31+G(d,p) and B3LYP/6-31+G(d,p) theoretical results[10] and are in good agreement with a mean relative deviation of less than 3.2%. Thus, the computed reaction energies for the $(NH_2)_2C{=}C(NO_2)(ONO) \rightarrow (NH_2)_2C{=}C(NO_2)O$ + NO reaction can be considered to be appropriate, and the double-hybrid density functionals are applicable for the evaluations of thermal rate constants in the present work.

Table 1 presents the relative thermodynamic properties of the stationary points to reactant on the potential energy surface for the CO−NO bond dissociation of $(NH_2)_2C{=}C(NO_2)(ONO)$. It is important that various single-reference methods provide very close transition-state energies (barrier height calculated by taking the energy difference between transition structure and reactant) and reaction energies. The activation energy value determined here is close to the estimate (61.1 kJ mol^{-1})[14] by the G4//B3LYP/6-311++G(3df,2p) level. It is clearly revealed that a low activation barrier is involved in the CO−NO bond fission. This is most likely due to the very small endothermicity (seen from Table 1) of forming a double bond between the carbon and oxygen atoms with the positive entropic effect, making the nitrite isomer of DADNE thermally unstable. The calculated reaction energy for the $(NH_2)_2C{=}C(NO_2)(ONO)$ dissociation reaction at 298.15 K in the present work, shown as in Table 1, concurs with the G4//B3LYP/6-311++G(3df,2p) result of 7.1 kJ mol^{-1},[14] which also confirms the reliability of our calculated results. Comparing the thermodynamic data of the postreaction adduct (IM) and separate products, one can see that IM is predicted to be lower in energy than $(NH_2)_2C{=}C(NO_2)O$ + NO by about 11−15 kJ mol^{-1}.

Rate Constants. The IRC follows the NO-loss pathway from $(NH_2)_2C{=}C(NO_2)(ONO)$. The B2PLYP/6-31G(d,p) calculated minimum potential energy (V_{MEP}), local zero-point vibrational energy (ZPE), and vibrationally adiabatic ground-

https://doi.org/10.1021/acsomega.1c01616
ACS Omega 2021, 6, 15292−15299

state potential energy (V_a^G) along the reaction coordinate (s) for the CO−NO bond dissociation of $(NH_2)_2C{=}C(NO_2)$-(ONO) are depicted in Figure 5.

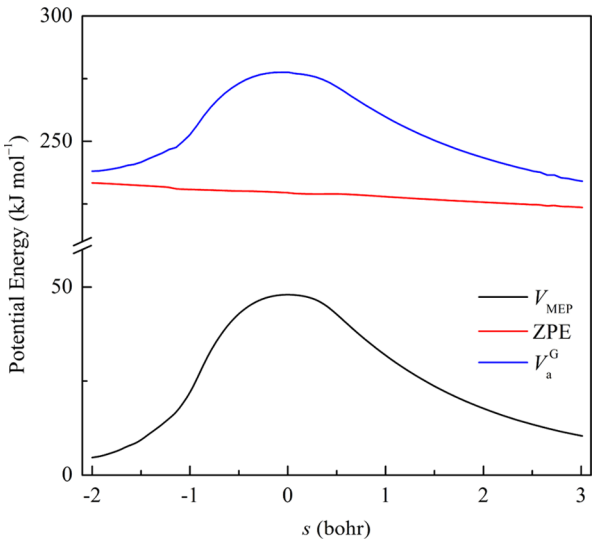

Figure 5. B2PLYP/6-31G(d,p) minimum-energy path potential $V_{MEP}(s)$, ZPE(s), and vibrationally adiabatic ground-state potential $V_a^G(s)$ profiles for the CO−NO bond dissociation of $(NH_2)_2C{=}C(NO_2)(ONO)$.

Location s corresponds to the distance along the MEP with s = 0 at TS. MEP terminates on the reactant side for a negative s and on the product side for a positive s. The $V_{MEP}(s)$ value representing the potential energy at location s relative to *trans*-$(NH_2)_2C{=}C(NO_2)(ONO)$ ($V_{MEP}(s \rightarrow -\infty) = 0$) is not corrected for the zero-point energy. ZPE(s) is computed with the B2PLYP/6-31G(d,p)-based Hessian data scaled by a factor of 0.9932, and $V_a^G(s)$ is obtained by adding ZPE(s) to $V_{MEP}(s)$. In addition, the T1 diagnostic was carried out for each stationary point on the MEP. Here, it should be noted that at high potential energies, there are a small number of points with larger T1 data than the cutoff T1 value for the open-shell systems, and they are not included in the data for fitting the V_{MEP}.

As shown in Figure 5, a barrier divides $(NH_2)_2C{=}C(NO_2)(ONO)$ and IM. For the CO−NO bond dissociation of $(NH_2)_2C{=}C(NO_2)(ONO)$, the significant geometry variations primarily occurs in the reaction coordinate range from −1.5 to 2.0 bohr, as seen from $V_{MEP}(s)$ in Figure 5, followed by the rearrangement of heavy atoms to form the $(NH_2)_2C{=}C(NO_2)(ONO)$ or IM structures, respectively. It can be found that the ZPE values decrease gradually with the reaction coordinate from the ZPE(s) profile.

The TST, CVT, and ICVT rate constants are calculated using the B2PLYP/6-31G(d,p)-based geometries, gradients, force constants, and energetics with the ZCT and SCT tunneling probabilities included. Here, it is worth noting that the overall rotational symmetry number for a given species has been included in its partition function approximations. The partition functions Q used in the rate constant calculations are approximated on the assumption of separability of electronic, translational, rotational, and vibrational contributions. All nonimaginary vibrational modes are treated as harmonic oscillators, and their partition functions are estimated by

$$Q_{vib,i}^{HO} = \frac{\exp(-h\omega_i(2k_BT))}{1 - \exp(-h\omega_i/(k_BT))} \quad (1)$$

where ω_i is the B2PLYP/6-31G(d,p) calculated frequency scaled by a factor of 0.9932 for the ith vibrational mode. In addition, the anharmonic effect of hindered torsions is not included in the rate constant calculations. Exclusion of torsional effect is to benefit from the cancellation of errors due to the conservation of similar types of internal rotations in the reactant $(NH_2)_2C{=}C(NO_2)(ONO)$ and transition-state geometries.

The calculated TST, CVT, ICVT, CVT/ZCT, and CVT/SCT rate constants at temperatures from 200 to 3000 K are outlined in Table 2, where /ZCT or /SCT denotes that the ZCT or SCT tunneling approximations are included in the rate constants. The TST rate constants overpredict the CVT values in the studied temperature range, and the difference between the TST and CVT rate constants increases with temperature, such as factors of k^{TST} to k^{CVT} are estimated to be 1.01, 1.49, 1.61, and 1.89, respectively, at 200, 1000, 2000, and 3000 K. The variational transition states move toward negative from s = −0.006 bohr at 200 K to locations s = −0.215 bohr at 1000 K and s equal to −0.256 bohr at 2000 K. At 3000 K, the

Table 2. Thermal Rate Constants in s^{-1} for the CO−NO Bond Dissociation of $(NH_2)_2C{=}C(NO_2)(ONO)$

T (K)	k^{TST}	k^{CVT}	k^{ICVT}	$k^{CVT/ZCT}$	$k^{CVT/SCT}$
200	1.460×10^{3}	1.450×10^{3}	1.450×10^{3}	1.224×10^{4}	6.382×10^{5}
250	1.750×10^{5}	1.730×10^{5}	1.730×10^{5}	5.740×10^{5}	4.414×10^{6}
298.15	3.965×10^{6}	3.914×10^{6}	3.914×10^{6}	8.788×10^{6}	2.709×10^{7}
400	2.567×10^{8}	2.204×10^{8}	2.204×10^{8}	3.414×10^{8}	5.448×10^{8}
600	1.591×10^{10}	1.191×10^{10}	1.191×10^{10}	1.444×10^{10}	1.726×10^{10}
800	1.282×10^{11}	8.958×10^{10}	8.958×10^{10}	9.982×10^{10}	1.100×10^{11}
1000	4.514×10^{11}	3.030×10^{11}	3.030×10^{11}	3.247×10^{11}	3.451×10^{11}
1200	1.047×10^{12}	6.846×10^{11}	6.846×10^{11}	7.183×10^{11}	7.492×10^{11}
1400	1.913×10^{12}	1.227×10^{12}	1.227×10^{12}	1.271×10^{12}	1.311×10^{12}
1600	3.008×10^{12}	1.902×10^{12}	1.902×10^{12}	1.955×10^{12}	2.001×10^{12}
1800	4.279×10^{12}	2.676×10^{12}	2.676×10^{12}	2.734×10^{12}	2.785×10^{12}
2000	5.672×10^{12}	3.516×10^{12}	3.516×10^{12}	3.578×10^{12}	3.632×10^{12}
2200	7.145×10^{12}	4.397×10^{12}	4.397×10^{12}	4.460×10^{12}	4.516×10^{12}
2600	1.019×10^{13}	6.201×10^{12}	6.201×10^{12}	6.265×10^{12}	6.321×10^{12}
3000	1.323×10^{13}	7.005×10^{12}	7.005×10^{12}	7.059×10^{12}	7.107×10^{12}

https://doi.org/10.1021/acsomega.1c01616
ACS Omega 2021, 6, 15292−15299

variational transition state moves to location $s = -0.286$ bohr. Here, it can be argued that variational effects play an important role in the $(NH_2)_2C{=}C(NO_2)(ONO)$ dissociation reaction, and variational treatments should be included in the rate constant approximations. Furthermore, it is found that k^{CVT} is almost equal to k^{ICVT} over the entire temperature range of 200−3000 K, which implies that the microcanonical effect can be negligible.

The CVT rate constants are sensitive to the region near the transition state, and the ZCT and SCT tunneling contributions show strong dependencies not only on the barrier height but also on the barrier width and the reaction path curvature. At high temperatures, the CVT/SCT and CVT/ZCT rate constant profiles are very close to the CVT one. It can be argued that the tunneling effect at high temperatures is negligible as more $(NH_2)_2C{=}C(NO_2)(ONO)$ molecules react either by passage over the activated barrier or by vibrational tunneling close to barrier height. When the reaction temperature decreases, the ZCT and SCT tunneling contributions to the kinetic model become more and more significant, and most of the vinyl nitrite molecules react by passage through the activated barrier with little vibrational activation. Due to a lower activation barrier involved in the process $(NH_2)_2C{=}C(NO_2)(ONO) \rightarrow (NH_2)_2C{=}C(NO_2)O + NO$ compared to the CO−NO bond scission of vinyl nitrite,[15] a more important tunneling effect is observed. Because the SCT tunneling estimations consider the local reaction path curvature near the transition state, the CVT/SCT rate constants are calculated to be generally larger than the CVT/ZCT rate constants at the same temperature with $k^{CVT/SCT}$: $k^{CVT/ZCT}$ being 5.21, 1.06, 1.02, and 1.01 at 200, 1000, 2000, and 3000 K, respectively. It can lead to a conclusion that the small-curvature contributions play a critical role in the CO−NO bond dissociation of $(NH_2)_2C{=}C(NO_2)(ONO)$ at low temperatures. Because experimental information is not available for the dissociation of $(NH_2)_2C{=}C(NO_2)(ONO)$, this study will enable a more rigorous understanding of the reaction kinetic mechanism, thus facilitating a comparison between theory and future experiments to improve the chemical kinetic model for the DADNE decomposition.

The parameters in the four-parameter modified Arrhenius functional form, given by eq 3, are obtained by minimizing the root mean square residual (RMSR), which is given by

$$\mathrm{RMSR} = \left\{ \frac{1}{N} \sum_{i=1}^{N} \ln\left[\frac{k(T_i)}{k_M(p_1, p_2, p_3, p_4, T_i)} \right]^2 \right\}^{1/2} \quad (2)$$

where N is the total number of temperatures, $k(T_i)$ is the CVT/SCT calculated rate constant at temperature T_i, and $k_M(p_1, p_2, p_3, p_4, T_i)$ are the fitted rate constant value at T_i. The four parameters are as follows: frequency factor $A = 1.05 \times 10^{13}$ s^{-1}, $E = 27.80$ kJ mol^{-1}, $n = 0.39$, and $T_0 = 205.32$ K for the kinetic model of the $(NH_2)_2C{=}C(NO_2)(ONO)$ dissociation.

CONCLUSIONS

Computational theoretical chemistry is employed to gain insights into the kinetic mechanism for the CO−NO dissociation of the nitrite isomer of DADNE to produce $(NH_2)_2C{=}C(NO_2)O + NO$. The calculated results presented in this paper indicate that the title reaction involves a well-defined saddle point directly connected to a hydrogen-bonded complex $(NO_2)C{=}C(NH_2)NH{\cdots}H{\cdots}NO$, which lies lower than the separate products $(NH_2)_2C{=}C(NO_2)O$ and NO in energy, and the activation energy at 298.15 K for the CO−NO dissociation of the nitrite isomer is calculated to be 43.6 kJ mol^{-1} at the B2PLYP/6-31G(d,p) level. For the computed rate constants, the tunneling effect appears to be important at low temperatures and variational effects are observed to be significant. The four-parameter modified Arrhenius form is employed to describe the temperature dependence of the CVT/SCT rate constants in the temperature range of 200−3000 K based on the B2PLYP/6-31G(d,p) geometries, gradients, force constants, and energetics. Note that some strong features proposed by our calculations have not been observed, and additional experiments seem to be necessary to verify the predictions.

COMPUTATIONAL DETAILS

Electronic Energy Calculations. Quantum chemical calculations were all executed with the Gaussian 09 suite of program.[21] In this work, double-hybrid density functionals (including B2PLYP,[22] B2PLYPD,[23] B2PLYPD3,[24,25] mPW2PLYP,[26] and mPW2PLYPD[23]) in conjunction with the 6-31G(d,p) basis set[27] were employed for the full geometry optimizations of reactant, product, intermediate, and transition state on the potential energy surface without symmetry restrictions. The double-hybrid density functionals have been verified to give accurate results of the molecular structures, vibrational frequencies, and kinetic parameters comparable to the CCSD(T)-based and experimental estimates.[23,28] Due to the limit of our computational resources, only the 6-31G(d,p) basis set, which did not require a lot of computer time, was adopted in the present work. Spin-restricted treatment was employed for the closed-shell species, $(NH_2)_2C{=}C(NO_2)(ONO)$, while the unrestricted method was applicable for NO and $(NH_2)_2C{=}C(NO_2)O$ radicals, postreaction adducts $(NH_2)_2C{=}C(NO_2)O{\cdots}NO$ (IM), and transition state (TS). Their wave function instability has been investigated.

Vibrational frequencies, summarized in the Supporting Information, have been calculated using the same theoretical level as optimizations for the characterization of the nature of stationary points and the determination of zero-point vibrational energies (ZPEs). All of the optimized geometries have been identified for minimum energy with no imaginary frequencies and the transition state with only one imaginary frequency, i.e., 536i cm^{-1} at the B2PLYP level and 580i cm^{-1} at the mPW2PLYP level, corresponding to the breaking and forming processes for the CO−NO bond of $(NH_2)_2C{=}C(NO_2)(ONO)$. A scaling factor of 0.9932 was applied to the B2PLYP/6-31G(d,p) harmonic frequencies to partially account for anharmonic effects.[29] In addition, the scale factors for the frequencies obtained at the B2PLYPD, B2PLYPD3, mPW2PLYP, and mPW2PLYPD levels with the 6-31G(d,p) basis set were the same as that for the B2PLYP/6-31G(d,p) ones.

Minimum-energy path (MEP) was traced using the intrinsic reaction coordinate (IRC) algorithm[30,31] with a step size of 0.02 bohr to check the energy profiles connecting the transition states to the two desirable minima: $(NH_2)_2C{=}C(NO_2)(ONO)$ and $(NH_2)_2C{=}C(NO_2)O{\cdots}NO$. The rate constant calculations were based on the B2PLYP/6-31G(d,p) gradients and Hessian of 60 selected points (24 and 36 points on the reactant and product sides, respectively) on the MEP.

https://doi.org/10.1021/acsomega.1c01616
ACS Omega 2021, 6, 15292−15299

The global electron density transfer (GEDT) at the transition state was computed by sharing the natural charges evaluated by the natural bond orbital (NBO) method[32,33] to evaluate the nonpolar or polar character of the reaction.[34,35] The extension in the bond formation at the stationary points was provided by the Wiberg bond order (WBO).[36]

Rate Constant Calculations. The high-pressure thermal rate constants with temperature were calculated by the conventional transition-state theory (TST),[37,38] canonical variational TST (CVT),[39] and improved CVT (ICVT)[40,41] using the Polyrate 9.7 program[42] with the inputs of the B2PLYP/6-31G(d,p)-based structures, energies, gradients, and force constants of the adopted points along the MEP. To include the quantum mechanical effects, the TST, CVT, and ICVT rate constants were improved by a temperature-dependent tunneling factor, $\kappa(T)$, which was estimated by the multidimensional zero-curvature tunneling (ZCT)[41] and small-curvature tunneling (SCT)[43] methods.

In the temperature range of 200−3000 K, the CVT/SCT rate constants calculated discretely every 50 K for the $(NH_2)_2C{=}C(NO_2)(ONO) \rightarrow (NH_2)_2C{=}C(NO_2)O + NO$ reaction were fitted to the following modified Arrhenius form[44]

$$k(T) = A\left(\frac{T}{300}\right)^{n} \exp\left(\frac{-E(T + T_0)}{R(T^2 + T_0^2)}\right) \quad (3)$$

where A, n, T_0, and E are the parameters of the modified Arrhenius equation.

■ ASSOCIATED CONTENT

Supporting Information

The Supporting Information is available free of charge at https://pubs.acs.org/doi/10.1021/acsomega.1c01616.

Part I: Table S1. Total and relative energies of the stationary points involved in the cis−trans interconversion of the nitrite isomer of DADNE. Table S2. Selected geometric parameters for $(NH_2)_2C{=}C(NO_2)(ONO)$, transition state (TS), intermediate (IM), $(NH_2)_2C{=}C(NO_2)O$, and NO. Table S3. T1 diagnostics (from the CCSD/6-31+G(d,p) calculations) and $\langle S^2 \rangle$ values (for open-shell species) of all species involved in the CO−NO bond dissociation of $(NH_2)_2C{=}C(NO_2)(ONO)$. Part II: Electronic geometries, unscaled frequencies, and rotational constants for all optimized stationary points at the B2PLYP, B2PLYPD, B2PLYPD3, mPW2PLYP, and mPW2PLYPD levels with the 6-31G(d,p) basis set (PDF)

■ AUTHOR INFORMATION

Corresponding Author

Yulei Guan − *School of Chemical Engineering/Xi'an Key Laboratory of Special Energy Materials, Northwest University, Xi'an 710069, China;* orcid.org/0000-0002-0494-8259; Phone: +86-29-88302632; Email: guanyl@nwu.edu.cn; Fax: +86-29-88307755

Authors

Xingzhen Zhu − *School of Chemical Engineering/Xi'an Key Laboratory of Special Energy Materials, Northwest University, Xi'an 710069, China*

Yanyan Gao − *School of Chemical Engineering/Xi'an Key Laboratory of Special Energy Materials, Northwest University, Xi'an 710069, China*

Haixia Ma − *School of Chemical Engineering/Xi'an Key Laboratory of Special Energy Materials, Northwest University, Xi'an 710069, China;* orcid.org/0000-0001-9080-2004

Jirong Song − *School of Chemical Engineering/Xi'an Key Laboratory of Special Energy Materials, Northwest University, Xi'an 710069, China*

Complete contact information is available at: https://pubs.acs.org/10.1021/acsomega.1c01616

Notes

The authors declare no competing financial interest.

■ ACKNOWLEDGMENTS

Financial support of this work by the National Natural Science Foundation of China (No. 21606178) and the Natural Science Foundation of Shaanxi Province of China (No. 2021JM-308) is gratefully acknowledged.

■ REFERENCES

(1) Klapötke, T. M. New Nitrogen-Rich High Explosives. In *Structure and Bonding*; 2007; Vol. *125*, pp 85−121.

(2) Gao, H. X.; Shreeve, J. M. Azole-Based Energetic Salts. *Chem. Rev.* **2011**, *111*, 7377−7436.

(3) Dippold, A. A.; Klapotke, T. M. A Study of Dinitro-bis-1,2,4-triazole-1,1′-diol and Derivatives: Design of High-Performance Insensitive Energetic Materials by the Introduction of N-Oxides. *J. Am. Chem. Soc.* **2013**, *135*, 9931−9938.

(4) Latypov, N. V.; Bergman, J.; Langlet, A.; Wellmar, U.; Bemm, U. Synthesis and Reactions of 1,1-Diamino-2,2-Dinitroethylene. *Tetrahedron* **1998**, *54*, 11525−11536.

(5) Trzcinski, W. A.; Cudzilo, S.; Chylek, Z.; Szymanczyk, L. Detonation Properties of 1,1-Diamino-2,2-Dinitroethene (DADNE). *J. Hazard. Mater.* **2008**, *157*, 605−612.

(6) Rashkeev, S. N.; Kuklja, M. M.; Zerilli, F. J. Electronic Excitations and Decomposition of 1,1-Diamino-2,2-Dinitroethylene. *Appl. Phys. Lett.* **2003**, *82*, 1371−1373.

(7) Kuklja, M. M.; Rashkeev, S. N.; Zerilli, F. J. Shear-Strain Induced Decomposition of 1,1-Diamino-2,2-Dinitroethylene. *Appl. Phys. Lett.* **2006**, *89*, No. 071904.

(8) de Klerk, W. P. C.; Popescu, C.; van der Heijden, A. Study on the Decomposition Kinetics of FOX-7 and HNF. *J. Therm. Anal. Calorim.* **2003**, *72*, 955−966.

(9) Politzer, P.; Concha, M. C.; Grice, M. E.; Murray, J. S.; Lane, P.; Habibollazadeh, D. Computational Investigation of the Structures and Relative Stabilities of Amino/Nitro Derivatives of Ethylene. *J. Mol. Struct.: Theochem* **1998**, *452*, 75−83.

(10) Gindulytė, A.; Massa, L.; Huang, L.; Karle, J. Proposed Mechanism of 1,1-Diamino-Dinitroethylene Decomposition: A Density Functional Theory Study. *J. Phys. Chem. A* **1999**, *103*, 11045−11051.

(11) Kimmel, A. V.; Sushko, P. V.; Shluger, A. L.; Kuklja, M. M. Effect of Charged and Excited States on the Decomposition of 1,1-Diamino-2,2-Dinitroethylene Molecules. *J. Chem. Phys.* **2007**, *126*, No. 234711.

(12) Kiselev, V. G.; Gritsan, N. P. Unexpected Primary Reactions for Thermolysis of 1,1-Diamino-2,2-dinitroethylene (FOX-7) Revealed by ab initio Calculations. *J. Phys. Chem. A* **2014**, *118*, 8002−8008.

(13) Yuan, B.; Yu, Z.; Bernstein, E. R. Initial Decomposition Mechanism for the Energy Release from Electronically Excited Energetic Materials: FOX-7 (1,1-Diamino-2,2-Dinitroethene, $C_2H_4N_4O_4$). *J. Chem. Phys.* **2014**, *140*, No. 074708.

(14) Booth, R. S.; Butler, L. J. Thermal Decomposition Pathways for 1,1-Diamino-2,2-Dinitroethene (FOX-7). *J. Chem. Phys.* **2014**, *141*, No. 134315.

(15) Guan, Y.; Lou, J.; Ma, H.; Song, J. Investigation on the Thermal Dissociation of Vinyl Nitrite with a Saddle Point Involved. *ACS Omega* **2019**, *4*, 16052−16061.
(16) Hirshfeld, F. L. Bonded-atom Fragments for Describing Molecular Charge Densities. *Theor. Chem. Acc.* **1977**, *44*, 129−138.
(17) Lee, T. J.; Taylor, P. R. A Diagnostic for Determining the Quality of Single-Reference Electron Correlation Methods. *Int. J. Quantum Chem.* **1989**, *23*, 199−207.
(18) Purvis, G. D., III; Bartlett, R. J. A Full Coupled-Cluster Singles and Doubles Model: The Inclusion of Disconnected Triples. *J. Chem. Phys.* **1982**, *76*, 1910−1918.
(19) Scuseria, G. E.; Janssen, C. L.; Schaefer, H. F., III An Efficient Reformulation of the Closed-Shell Coupled Cluster Single and Double Excitation (CCSD) Equations. *J. Chem. Phys.* **1988**, *89*, 7382−7387.
(20) Alecu, I. M.; Truhlar, D. G. Computational Study of the Reactions of Methanol with the Hydroperoxyl and Methyl Radicals. 1. Accurate Thermochemistry and Barrier Heights. *J. Phys. Chem. A* **2011**, *115*, 2811−2829.
(21) Frisch, M. J.; Trucks, G. W.; Schlegel, H. B.; Scuseria, G. E.; Robb, M. A.; Cheeseman, J. R.; Scalmani, G.; Barone, V.; Mennucci, B.; Petersson, G. A.. et al.*Gaussian 09*, Revision A.02; Gaussian, Inc.: Wallingford, CT, 2009.
(22) Grimme, S. Semiempirical Hybrid Density Functional with Perturbative Second-Order Correlation. *J. Chem. Phys.* **2006**, *124*, 034108/1−16.
(23) Schwabe, T.; Grimme, S. Double-Hybrid Density Functionals with Long-Range Dispersion Corrections: Higher Accuracy and Extended Applicability. *Phys. Chem. Chem. Phys.* **2007**, *9*, 3397−3406.
(24) Grimme, S.; Antony, J.; Ehrlich, S.; Krieg, H. A Consistent and Accurate ab initio Parametrization of Density Functional Dispersion Correction (DFT-D) for the 94 Elements H-Pu. *J. Chem. Phys.* **2010**, *132*, No. 154104.
(25) Grimme, S. Density Functional Theory with London Dispersion Corrections. *Wiley Interdiscip. Rev.: Comput. Mol. Sci.* **2011**, *1*, 211−228.
(26) Schwabe, T.; Grimme, S. Towards Chemical Accuracy for the Thermodynamics of Large Molecules: New Hybrid Density Functionals Including Non-Local Correlation Effects. *Phys. Chem. Chem. Phys.* **2006**, *8*, 4398−4401.
(27) Frisch, M. J.; Pople, J. A.; Binkley, J. S. Self-consistent Molecular Orbital Methods 25. Supplementary Functions for Gaussian Basis Set. *J. Chem. Phys.* **1984**, *80*, 3265−3269.
(28) Biczysko, M.; Panek, P.; Scalmani, G.; Bloino, J.; Barone, V. Harmonic and Anharmonic Vibrational Frequency Calculations with the Double-Hybrid B2PLYP Method: Analytic Second Derivatives and Benchmark Studies. *J. Chem. Theory Comput.* **2010**, *6*, 2115−2125.
(29) Kesharwani, M. K.; Brauer, B.; Martin, J. M. L. Frequency and Zero-Point Vibrational Energy Scale Factors for Double-Hybrid Density Functionals (and Other Selected Methods): Can Anharmonic Force Fields be Avoided? *J. Phys. Chem. A* **2015**, *119*, 1701−1714.
(30) Hratchian, H. P.; Schlegel, H. B. Accurate Reaction Paths Using a Hessian Based Predictor-Corrector Integrator. *J. Chem. Phys.* **2004**, *120*, 9918−9924.
(31) Hratchian, H. P.; Schlegel, H. B. Using Hessian Updating to Increase the Efficiency of a Hessian Based Predictor-Corrector Reaction Path Following Method. *J. Chem. Theory Comput.* **2005**, *1*, 61−69.
(32) Reed, A. E.; Weinstock, R. B.; Weinhold, F. Natural Population Analysis. *J. Chem. Phys.* **1985**, *83*, 735−746.
(33) Reed, A. E.; Curtiss, L. A.; Weinhold, F. Intermolecular Interactions from a Natural Bond Orbital, Donor-Acceptor Viewpoint. *Chem. Rev.* **1988**, *88*, 899−926.
(34) Domingo, L. R. A New C−C Bond Formation Model Based on the Quantum Chemical Topology of Electron Density. *RSC Adv.* **2014**, *4*, 32415−32428.
(35) Jasiński, R.; Jasińska, E.; Dresler, E. A DFT Computational Study of the Molecular Mechanism of [3 + 2] Cycloaddition Reactions between Nitroethene and Benzonitrile *N*-oxides. *J. Mol. Model.* **2017**, *23*, 13.
(36) Wiberg, K. B. Application of the Pople-santry-segal CNDO Method to the Cyclopropylcarbinyl and Cyclobutyl Cation and to Bicyclobutane. *Tetrahedron* **1968**, *24*, 1083−1096.
(37) Eyring, H. The Activated Complex and the Absolute Rate of Chemical Reactions. *Chem. Rev.* **1935**, *17*, 65−77.
(38) Laidler, K. J.; King, M. C. The Development of Transition-State Theory. *J. Phys. Chem. A* **1983**, *87*, 2657−2664.
(39) Garrett, B. C.; Truhlar, D. G. Generalized Transition State Theory. Bond Energy-Bond Order Method for Canonical Variational Calculations with Application to Hydrogen Atom Transfer Reactions. *J. Am. Chem. Soc.* **1979**, *101*, 4534−4548.
(40) Truhlar, D. G.; Garrett, B. C. Variational Transition-State Theory. *Acc. Chem. Res.* **1980**, *13*, 440−448.
(41) Garrett, B. C.; Truhlar, D. G.; Grev, R. S.; Magnuson, A. W. Improved Treatment of Threshold Contributions in Variational Transition-State Theory. *J. Phys. Chem. A* **1980**, *84*, 1730−1748.
(42) Corchado, J. C.; Chuang, Y.-Y.; Fast, P. L.; Hu, W.-P.; Liu, Y.-P.; Lynch, G. C.; Nguyen, K. A.; Jackels, C. F.; Ramos, A. F.; Ellingson, B. A.; Lynch, B. J.; Zheng, J.-J.; Melissas, V. S.; Villà, J.; Rossi, I.; Coitino, E. L.; Pu, J.-Z.; Albu, T. V.; Steckler, R.; Garrett, B. C.; Isaacson, A. D.; Truhlar, D. G. *Polyrate 9.7*; University of Minnesota: Minneapolis, Minnesota, USA, 2007.
(43) Liu, Y.-P.; Lynch, G. C.; Truong, T. N.; Lu, D.-H.; Truhlar, D. G.; Garrett, B. C. Molecular Modeling of the Kinetic Isotope Effect for the [1,5] Sigmatropic Rearrangement of *cis*-1,3-Pentadiene. *J. Am. Chem. Soc.* **1993**, *115*, 2408−2415.
(44) Zheng, J.; Truhlar, D. G. Kinetics of Hydrogen-Transfer Isomerizations of Butoxyl Radicals. *Phys. Chem. Chem. Phys.* **2010**, *12*, No. 7782.

https://doi.org/10.1021/acsomega.1c01616
ACS Omega 2021, 6, 15292−15299